A. B. M. Tahidul Haque
Department of Civil, Structural and Environmental Engineering,
University at Buffalo,
116 Ketter Hall,
Buffalo, NY 14260

Ratiba F. Ghachi
Department of Civil and Architectural Engineering,
Qatar University,
Doha 2713, Qatar

Wael I. Alnahhal
Department of Civil and Architectural Engineering,
Qatar University,
Doha 2713, Qatar

Amjad Aref
Department of Civil, Structural and Environmental Engineering,
University at Buffalo,
235 Ketter Hall,
Buffalo, NY 14260

Jongmin Shim[1]
Department of Civil, Structural and Environmental Engineering,
University at Buffalo,
240 Ketter Hall,
Buffalo, NY 14260
e-mail: jshim@buffalo.edu

Generalized Spatial Aliasing Solution for the Dispersion Analysis of Infinitely Periodic Multilayered Composites Using the Finite Element Method

The finite element (FE) method offers an efficient framework to investigate the evolution of phononic crystals which possess materials or geometric nonlinearity subject to external loading. Despite its superior efficiency, the FE method suffers from spectral distortions in the dispersion analysis of waves perpendicular to the layers in infinitely periodic multilayered composites. In this study, the analytical dispersion relation for sagittal elastic waves is reformulated in a substantially concise form, and it is employed to reproduce spatial aliasing-induced spectral distortions in FE dispersion relations. Furthermore, through an anti-aliasing condition and the effective elastic modulus theory, an FE modeling general guideline is provided to overcome the observed spectral distortions in FE dispersion relations of infinitely periodic multilayered composites, and its validity is also demonstrated. [DOI: 10.1115/1.4036469]

1 Introduction

In various elastodynamic wave propagation disciplines, layered composites have recently gained popularity. Some widespread uses of bilayered composites are found in acoustic waveguide [1], acoustic rectifier [2], tunable piezoelectric materials [3], and nanostructured polymer layers [4]. In addition, multilayered composites having more than two layers per unit cell are being heavily investigated for various potential applications, which include stress-wave attenuation [5], acoustic rectification [6], negative effective dynamic properties [7,8], etc. Such novel applications of layered composites are mainly due to the phononic band-gap property of their dispersion relation.

The analytical dispersion relation for wave propagation perpendicular to the layers has been investigated thoroughly for both infinitely periodic bilayered composites [9–14] and infinitely periodic multilayered composites [15–17]. On the other hand, due to the complexity of the configuration, there have been limited analytical investigations on dispersion relation for wave motion at arbitrary angles in the sagittal plane, in which the pressure wave (P-wave) and vertical shear wave (SV-wave) propagate [18]. The analytical dispersion relations of infinitely periodic bilayered composites for sagittal plane waves can be found in several references [18–21]. However, only a few researchers [22,23] have presented the analytical dispersion relation of infinitely periodic multilayered composites for the sagittal plane waves, and their formulations are unduly complex.

In order to overcome the challenges in the analytical investigations, researchers have been employing various numerical techniques such as continuum power series method [24,25], the effective stiffness method [26,27], the mixture theory [28–30], the plane wave expansion method [31], the finite difference method [32], the variational method [33,34], and the finite element (FE) method [35–39]. In particular, the FE method offers a remarkable framework to efficiently investigate the effect of material and geometric nonlinearity on phononic dispersion relations [38,40–43], which can be hardly done using other numerical techniques. So, it has become a prevalent method to study the evolution of phononic dispersion relations due to the effect of nonlinearities of structures. In the FE method, a two-step manner is typically employed to study the evolution of dispersion relation of a periodic composite subject to external loading. The first step is a conventional static nonlinear analysis on the periodic composite, and this step considers material and geometric nonlinearities in the FE framework. In the second step, a linear perturbation analysis is performed on the deformed periodic composite to obtain dispersion relations, which is the subject matter of this manuscript. Through this procedure, researchers in the FE community have opened the possibility of tuning the band-structure of periodic structures [38,40,42,44,45].

However, despite its superior capability to investigate the effect of nonlinearities to phononic dispersion relations, the FE method suffers from spectral distortions in the dispersion analysis of waves perpendicular to the layers in layered composites [35–39]. The importance of this issue regarding FE modeling and the corresponding analysis are extensively discussed in Refs. [35] and [46]. It is worth mentioning that the spectral distortion discussed in those references is irrelevant to the effect of mesh size in FE models. It is ironic that the numerical technique (i.e., FE method) suitable for complex phononic calculations cannot properly handle

[1]Corresponding author.

Contributed by the Technical Committee on Vibration and Sound of ASME for publication in the JOURNAL OF VIBRATION AND ACOUSTICS. Manuscript received September 26, 2016; final manuscript received March 28, 2017; published online June 28, 2017. Assoc. Editor: Matthew Brake.

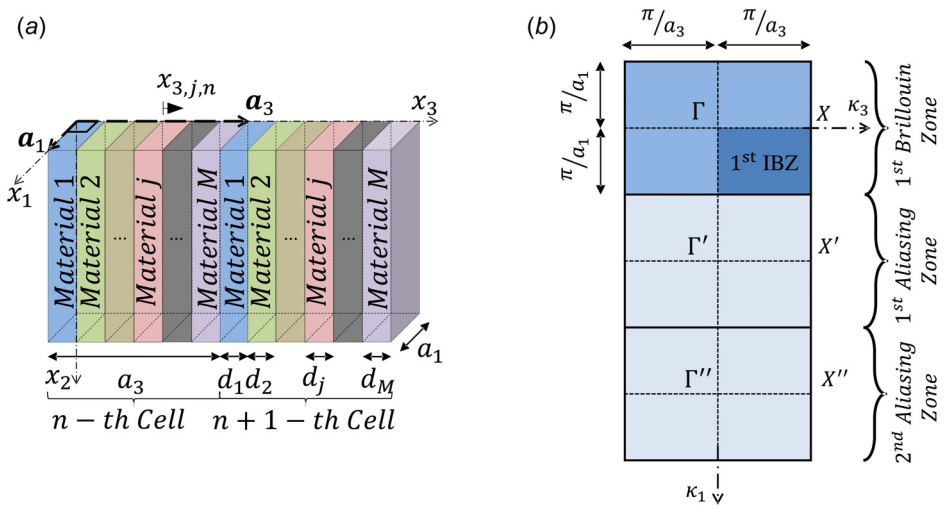

Fig. 1 (*a*) Geometry of a multilayered periodic composite, whose unit cell is spanned by primitive lattice vectors $\mathbf{a}_1$ and $\mathbf{a}_3$ in a two-dimensional (2D) coordinate space. Note that $a_1 = ||\mathbf{a}_1||$ and $a_3 = ||\mathbf{a}_3||$. (*b*) The corresponding wavevector space, where the topmost rectangle delineated by a thick solid line represents first Brillouin zone. Note that the aliasing paths are denoted by thick dotted lines.

the simplest geometry in phononic crystals (i.e., infinitely periodic layered composites). Simple geometries such as, spring-dashpot models [47] or one-dimensional (1D) granular crystals [48] have been adopted to investigate the effect of damping or nonlinearity in phononic structures. Without resolving this critical issue in FE dispersion relations, the FE method cannot be properly applied to investigate the effect of material nonlinearity on the phononic dispersion relation of infinitely periodic multilayered composites. Specifically, the structural 1D elements (e.g., truss or beam elements) available in the FE method are not suited for the dispersion analysis of infinitely periodic layered composites because an infinite length in the direction parallel to the layers (i.e., x_1 direction in Fig. 1(*a*)) cannot be considered in such elements. Thus, researchers in the FE community have to adopt 2D elements and apply the redundant Bloch periodic condition along the direction parallel to the layers [35–39]. For infinitely periodic *bilayered* composites, we recently showed that the spectral distortions are attributed to the spatial aliasing stemming from the use of 2D rectangular unit cell and proposed a FE modeling guideline to avoid this issue in the dispersion relation of waves perpendicular to the layers [46].

Furthermore, we revisit the analytical dispersion relation of infinitely periodic multilayered composites for waves in the sagittal plane, and newly derive the analytical solution in a notably concise form. We adopt the transfer matrix approach to investigate the multilayered composite problem in a simple, systematic way. The derived analytical solution is employed to reproduce fictitious modes in FE dispersion relations, which originate from the inevitable usage of 2D unit cell in the FE modeling of infinitely periodic multilayered composites. Moreover, we offer a generalized FE modeling guideline for infinitely periodic multilayered composites to avoid the spectral distortions within a frequency range of interest.

2 Analytical Dispersion Relations for Multilayered Periodic Composites

For infinitely periodic multilayered composites, only a few researchers [22,23] have presented the analytical dispersion relation of sagittal plane waves. For instance, Nayfeh derived an analytical solution, which is based on a linear transformation adopting the transformation matrix approach [22]. Moreover, Braga and Herrmann presented a solution based on a sextic formalism using a variation of transformation matrix [23]. However, due to their unduely complex formulations, it is challenging to have an insightful physical interpretation in the adopted derivation procedures and their outcomes. Note that the derivation presented in this paper is completely independent of the previous works [22,23] although we adopted the traditional transfer matrix approach together with the Bloch theorem. In this section, the analytical formulation of sagittal plane waves is first revisited, and its surprisingly concise form is derived by obtaining a transfer matrix, whose expression has not been reported in the literature. Then, the dispersion relation of wave propagation perpendicular to the layers is obtained through the similar approach.

Consider an infinitely periodic multilayered composite which has a periodic length a_3 along the x_3-axis (see Fig. 1(*a*)). Each unit cell consists of M layers, and the thickness of the jth layer is denoted by d_j, so that $a_3 = \sum_{j=1}^{M} d_j$. For the jth layer, the mass density of its material is denoted by ρ_j, and the elastic properties are given by $c_{11,j} = \lambda_j + 2\mu_j$, $c_{44,j} = \mu_j$ and $c_{12,j} = c_{11,j} - 2c_{44,j} = \lambda_j$, where λ_j and μ_j are Lamé constants. Furthermore, the pressure and shear wave velocities in the jth layer are denoted by $c_{p,j} = \sqrt{c_{11,j}/\rho_j}$ and $c_{s,j} = \sqrt{c_{44,j}/\rho_j}$, respectively.

2.1 Wave Propagation at Arbitrary Angle in the Sagittal Plane.

In the sagittal plane (i.e., the x_1–x_3 plane shown in Fig. 1(*a*)), the displacement field should be a function of x_1, x_3, and t. Consequently, the dispersion relation for sagittal plane waves should be described in a three-dimensional plot, i.e., ω over the κ_1–κ_3 plane. The irreducible Brillouin zone (IBZ) [49] can be determined by considering the symmetry of the layered composite, and it results in wavevector domain of $\kappa_1 \in [0, \infty)$ and $\kappa_3 \in [0, \pi/a_3]$ (see Fig. 1(*b*)). For a fixed κ_1, we first solve the governing equation with boundary conditions. Then, the complete picture of the dispersion relation over the κ_1–κ_3 plane is obtained by sweeping κ_1 over the range of $[0, \infty)$.

Using the Helmholtz's decomposition [50], the displacement field $\mathbf{u}$ is resolved into the sum of the contribution from a dilatation-related scalar potential Φ and the contribution from a rotation-related vector potential $\mathbf{H} = [H_1\, H_2\, H_3]^{\mathrm{T}}$, i.e., $\mathbf{u} = \nabla\Phi + \nabla \times \mathbf{H}$ and $\nabla \cdot \mathbf{H} = 0$. Consequently, the governing equations of motion are decomposed into sagittal plane waves (i.e., P- and SV-waves) and antiplane shear waves (i.e., SH-wave) [18,50].

Specifically, the governing equations of motion for coupled P- and SV-wave propagations in the sagittal plane can be

expressed in terms of Φ and H_2. For the jth layer of nth unit cell, the displacement components relating to sagittal plane waves are expressed by

$$u_{1,j,n}(x_1, x_{3,j,n}, t) = \frac{\partial \Phi_j}{\partial x_1} + \frac{\partial H_{2,j}}{\partial x_{3,j,n}}$$
$$u_{3,j,n}(x_1, x_{3,j,n}, t) = \frac{\partial \Phi_j}{\partial x_{3,j,n}} - \frac{\partial H_{2,j}}{\partial x_1} \tag{1}$$

and the corresponding governing equations are given by

$$\frac{\partial^2 \Phi_j}{\partial x_{3,j,n}^2} + \frac{\partial^2 \Phi_j}{\partial x_1^2} = \frac{1}{c_{p,j}^2}\frac{\partial^2 \Phi_j}{\partial t^2}$$
$$\frac{\partial^2 H_{2,j}}{\partial x_{3,j,n}^2} + \frac{\partial^2 H_{2,j}}{\partial x_1^2} = \frac{1}{c_{s,j}^2}\frac{\partial^2 H_{2,j}}{\partial t^2} \tag{2}$$

where $x_{3,j,n}$ represents the local x_3-coordinate for the jth layer of nth unit cell (see Fig. 1(*a*)). Assuming harmonic plane waves in composites, the solutions of Eq. (2) are found to be

$$\Phi_j(x_1, x_{3,j,n}, t) = \hat{\phi}_{F,j} e^{i(\kappa_1 x_1 - \alpha_{p,j} x_{3,j,n} - \omega t)} + \hat{\phi}_{B,j} e^{i(\kappa_1 x_1 + \alpha_{p,j} x_{3,j,n} - \omega t)}$$
$$H_{2,j}(x_1, x_{3,j,n}, t) = \hat{h}_{F,j} e^{i(\kappa_1 x_1 - \alpha_{s,j} x_{3,j,n} - \omega t)} + \hat{h}_{B,j} e^{i(\kappa_1 x_1 + \alpha_{s,j} x_{3,j,n} - \omega t)} \tag{3}$$

where $\alpha_{p,j} = \sqrt{(\omega^2/c_{p,j}^2 - \kappa_1^2)}$ and $\alpha_{s,j} = \sqrt{(\omega^2/c_{s,j}^2 - \kappa_1^2)}$, and $\hat{\phi}_{F,j}$, $\hat{\phi}_{B,j}$, $\hat{h}_{F,j}$, and $\hat{h}_{B,j}$ are the unknown amplitudes (or coefficients) to be determined from boundary conditions at the layer interfaces. By substituting Eq. (3) into Eq. (1), we obtain an expression for the displacement **u**

$$\begin{aligned} u_{3,j,n}(x_1, x_{3,j,n}, t) = {} & (-i\alpha_{p,j}\hat{\phi}_{F,j}) e^{i(\kappa_1 x_1 - \alpha_{p,j} x_{3,j,n} - \omega t)} \\ & + (i\alpha_{p,j}\hat{\phi}_{B,j}) e^{i(\kappa_1 x_1 + \alpha_{p,j} x_{3,j,n} - \omega t)} \\ & + (-i\kappa_1 \hat{h}_{F,j}) e^{i(\kappa_1 x_1 - \alpha_{s,j} x_{3,j,n} - \omega t)} \\ & + (-i\kappa_1 \hat{h}_{B,j}) e^{i(\kappa_1 x_1 + \alpha_{s,j} x_{3,j,n} - \omega t)} \\ u_{1,j,n}(x_1, x_{3,j,n}, t) = {} & (i\kappa_1 \hat{\phi}_{F,j}) e^{i(\kappa_1 x_1 - \alpha_{p,j} x_{3,j,n} - \omega t)} \\ & + (i\kappa_1 \hat{\phi}_{B,j}) e^{i(\kappa_1 x_1 + \alpha_{p,j} x_{3,j,n} - \omega t)} \\ & + (-i\alpha_{s,j}\hat{h}_{F,j}) e^{i(\kappa_1 x_1 - \alpha_{s,j} x_{3,j,n} - \omega t)} \\ & + (i\alpha_{s,j}\hat{h}_{B,j}) e^{i(\kappa_1 x_1 + \alpha_{s,j} x_{3,j,n} - \omega t)} \end{aligned} \tag{4}$$

Here, in order to have decoupled pressure and shear motion in the case of wave propagation perpendicular to the layers (i.e., $\kappa_1 = 0$), the following simplified amplitudes are introduced:

$$P_{F,j,n} = -i\alpha_{p,j}\hat{\phi}_{F,j}, \quad P_{B,j,n} = i\alpha_{p,j}\hat{\phi}_{B,j}, \quad Q_{F,j,n} = -i\alpha_{s,j}\hat{h}_{F,j},$$
$$P_{B,j,n} = i\alpha_{s,j}\hat{h}_{B,j} \tag{5}$$

Using the simplified unknown amplitudes, the displacement of the jth layer in nth unit cell (i.e., $\mathbf{u}_{j,n}$) can be expressed as follows:

$$\begin{aligned} u_{3,j,n}(x_1, x_{3,j,n}, t) = {} & \left[P_{F,j,n} e^{-i\alpha_{p,j} x_{3,j,n}} + P_{B,j,n} e^{i\alpha_{p,j} x_{3,j,n}} + \frac{\kappa_1}{\alpha_{s,j}} Q_{F,j,n} e^{-i\alpha_{s,j} x_{3,j,n}} - \frac{\kappa_1}{\alpha_{s,j}} Q_{B,j,n} e^{i\alpha_{s,j} x_{3,j,n}}\right] e^{i(\kappa_1 x_1 - \omega t)} \\ u_{1,j,n}(x_1, x_{3,j,n}, t) = {} & \left[-\frac{\kappa_1}{\alpha_{p,j}} P_{F,j,n} e^{-i\alpha_{p,j} x_{3,j,n}} + \frac{\kappa_1}{\alpha_{p,j}} P_{B,j,n} e^{i\alpha_{p,j} x_{3,j,n}} + Q_{F,j,n} e^{-i\alpha_{s,j} x_{3,j,n}} + Q_{B,j,n} e^{i\alpha_{s,j} x_{3,j,n}}\right] e^{i(\kappa_1 x_1 - \omega t)} \end{aligned} \tag{6}$$

Furthermore, the corresponding stresses of the jth layer in nth unit cell are given by

$$\begin{aligned} \sigma_{33,j,n}(x_1, x_{3,j,n}, t) = {} & \left[-P_{F,j,n} \frac{c_{11,j}\alpha_{p,j}{}^2 + c_{12,j}\kappa_1^2}{\alpha_{p,j}} e^{-i\alpha_{p,j} x_{3,j,n}} + P_{B,j,n} \frac{c_{11,j}\alpha_{p,j}{}^2 + c_{12,j}\kappa_1^2}{\alpha_{p,j}} e^{i\alpha_{p,j} x_{3,j,n}} + Q_{F,j,n}(c_{12,j} - c_{11,j})\kappa_1 e^{-i\alpha_{s,j} x_{3,j,n}} \right. \\ & \left. + Q_{B,j,n}(c_{12,j} - c_{11,j})\kappa_1 e^{i\alpha_{s,j} x_{3,j,n}}\right] e^{i(\kappa_1 x_1 - \omega t)} \\ \sigma_{31,j,n}(x_1, x_{3,j,n}, t) = {} & \left[2P_{F,j,n} c_{44,j}\kappa_1 e^{-i\alpha_{p,j} x_{3,j,n}} + 2P_{B,j,n} c_{44,j}\kappa_1 e^{i\alpha_{p,j} x_{3,j,n}} + Q_{F,j,n} \frac{c_{44,j}(\kappa_1^2 - \alpha_{s,j}{}^2)}{\alpha_{s,j}} e^{-i\alpha_{s,j} x_{3,j,n}} \right. \\ & \left. - Q_{B,j,n} \frac{c_{44,j}(\kappa_1^2 - \alpha_{s,j}{}^2)}{\alpha_{s,j}} e^{i\alpha_{s,j} x_{3,j,n}}\right] e^{i(\kappa_1 x_1 - \omega t)} \end{aligned} \tag{7}$$

Eventually, the four unknown amplitudes $P_{F,j,n}$, $P_{B,j,n}$, $Q_{F,j,n}$, and $Q_{B,j,n}$ can be determined by applying two displacement and two stress boundary conditions at the layer interface between the jth and the $(j+1)$th layers in the nth unit cell

$$[u_{3,j,n}]_{x_{3,j,n}=d_j} = [u_{3,j+1,n}]_{x_{3,j+1,n}=0}, \quad [u_{1,j,n}]_{x_{3,j,n}=d_j} = [u_{1,j+1,n}]_{x_{3,j+1,n}=0}$$
$$[\sigma_{33,j,n}]_{x_{3,j,n}=d_j} = [\sigma_{33,j,n}]_{x_{3,j+1,n}=0}, \quad [\sigma_{31,j,n}]_{x_{3,j,n}=d_j} = [\sigma_{31,j,n}]_{x_{3,j+1,n}=0} \tag{8}$$

After successively applying the boundary conditions (8) at all the interfaces within the nth unit cell, one can eventually find that wave motion (represented by the amplitudes, $P_{F,j,n}$, $P_{B,j,n}$, $Q_{F,j,n}$, and $Q_{B,j,n}$) in the first layer of the nth unit cell is related to that in the first layer of the $(n+1)$th unit cells as follows:

$$\mathbf{W}_{s,1,n+1} = \mathbf{T}_s \mathbf{W}_{s,1,n} \tag{9}$$

where

$$\mathbf{W}_{s,1,n} = \begin{bmatrix} P_{F,1,n} \\ P_{B,1,n} \\ Q_{F,1,n} \\ Q_{B,1,n} \end{bmatrix}, \quad \mathbf{W}_{s,1,n+1} = \begin{bmatrix} P_{F,1,n+1} \\ P_{B,1,n+1} \\ Q_{F,1,n+1} \\ Q_{B,1,n+1} \end{bmatrix} \tag{10}$$

$$\mathbf{T}_s = \mathbf{R}_{s,1}^{-1}(\mathbf{R}_{s,M}\mathbf{D}_{s,M}\mathbf{R}_{s,M}^{-1})\ldots(\mathbf{R}_{s,2}\mathbf{D}_{s,2}\mathbf{R}_{s,2}^{-1})\mathbf{R}_{s,1}\mathbf{D}_{s,1} = \mathbf{R}_{s,1}^{-1}\left(\prod_{j=2}^{M}\mathbf{R}_{s,M+2-j}\mathbf{D}_{s,M+2-j}\mathbf{R}_{s,M+2-j}^{-1}\right)\mathbf{R}_{s,1}\mathbf{D}_{s,1} \tag{11}$$

$$\mathbf{R}_{s,j} = \begin{bmatrix} 1 & 1 & \dfrac{\kappa_1}{\alpha_{s,j}} & -\dfrac{\kappa_1}{\alpha_{s,j}} \\ -\dfrac{\kappa_1}{\alpha_{p,j}} & \dfrac{\kappa_1}{\alpha_{p,j}} & 1 & 1 \\ -\dfrac{c_{11,j}\alpha_{p,j}^2 + c_{12,j}\kappa_1^2}{\alpha_{p,j}} & \dfrac{c_{11,j}\alpha_{p,j}^2 + c_{12,j}\kappa_1^2}{\alpha_{p,j}} & (c_{12,j} - c_{11,j})\kappa_1 & (c_{12,j} - c_{11,j})\kappa_1 \\ 2c_{44,j}\kappa_1 & 2c_{44,j}\kappa_1 & \dfrac{c_{44,j}\left(\kappa_1^2 - \alpha_{s,j}^2\right)}{\alpha_{s,j}} & -\dfrac{c_{44,j}\left(\kappa_1^2 - \alpha_{s,j}^2\right)}{\alpha_{s,j}} \end{bmatrix} \tag{12}$$

$$\mathbf{D}_{s,j} = \begin{bmatrix} e^{-i\alpha_{p,j}d_j} & 0 & 0 & 0 \\ 0 & e^{i\alpha_{p,j}d_j} & 0 & 0 \\ 0 & 0 & e^{-i\alpha_{s,j}d_j} & 0 \\ 0 & 0 & 0 & e^{i\alpha_{s,j}d_j} \end{bmatrix} \tag{13}$$

where the subscript s stands for sagittal waves, and $\mathbf{T}_s$ denotes the transfer matrix which determines the relation between the amplitude vectors ($\mathbf{W}_{s,1,n}$ and $\mathbf{W}_{s,1,n+1}$) of adjacent unit cells in the sagittal plane.

Furthermore, we have another relation between the nth and $(n+1)$th unit cells from the Bloch-periodic condition [49]

$$\mathbf{W}_{s,1,n+1} = e^{i\kappa_3 a_3}\mathbf{W}_{s,1,n} \tag{14}$$

Now, by combining Eqs. (9) and (14), one can obtain an eigenvalue problem for sagittal plane waves at a given κ_1

$$\mathbf{T}_s\mathbf{W}_{s,1,n} = e^{i\kappa_3 a_3}\mathbf{W}_{s,1,n} \tag{15}$$

where $e^{i\kappa_3 a_3}$ and $\mathbf{W}_{s,1,n}$ are the eigenvalue and eigenvector of $\mathbf{T}_s$, respectively. For a given κ_1, the dispersion relation can be obtained by solving the above eigenvalue problem of κ_3. By setting $e^{i\kappa_3 a_3} = \lambda$, the characteristic polynomial equation of $\mathbf{T}_s$ can be obtained from the Cayley–Hamilton theorem [51]

$$\lambda^4 - g_3\lambda^3 + g_2\lambda^2 - g_1\lambda + g_0 = 0 \tag{16}$$

with

$$\begin{aligned} g_3(\omega,\kappa_1) &= \mathrm{tr}(\mathbf{T}_s) \\ g_2(\omega,\kappa_1) &= \frac{1}{2}\left[[\mathrm{tr}(\mathbf{T}_s)]^2 - \mathrm{tr}\left(\mathbf{T}_s^2\right)\right] \\ g_1(\omega,\kappa_1) &= \frac{1}{6}\left[[\mathrm{tr}(\mathbf{T}_s)]^3 - 3\,\mathrm{tr}(\mathbf{T}_s)\mathrm{tr}\left(\mathbf{T}_s^2\right) + 2\,\mathrm{tr}\left(\mathbf{T}_s^3\right)\right] \\ g_0(\omega,\kappa_1) &= \det(\mathbf{T}_s) \end{aligned} \tag{17}$$

where tr(□) and det(□) denote the trace and the determinant of a matrix, respectively. Here, the polynomial coefficients (g_1,…,g_4) can also be determined from four roots $\lambda_r = e^{i\kappa_{3,r}a_3}$ (with $r = 1,\ldots,4$) of Eq. (16). Recall that the dispersion relation is symmetric along κ_1- and κ_3-axes due to the symmetry of geometric configuration of infinitely periodic multilayered composites. Thus, for a given $\kappa_1 \in [0, \infty)$, only two out of four solutions provide distinctively different eigenmodes (denoted by $\kappa_{3,1}$ and $\kappa_{3,2}$), while the other two solutions are located at the symmetric position along κ_3-axis, i.e., $\kappa_{3,3} = -\kappa_{3,1}$ and $\kappa_{3,4} = -\kappa_{3,2}$. Consequently, the roots of the characteristic polynomial (16) retain the reciprocal relation, i.e., $\lambda_3 = 1/\lambda_1$ and $\lambda_4 = 1/\lambda_2$. Now, the polynomial coefficients $g_1(\omega, \kappa_1)$ and $g_0(\omega, \kappa_1)$ become simplified

$$\begin{aligned} g_1(\omega,\kappa_1) &= g_3(\omega,\kappa_1) = \mathrm{tr}(\mathbf{T}_s) \\ g_0(\omega,\kappa_1) &= 1 \end{aligned} \tag{18}$$

Finally, by solving the simplified characteristic polynomial equation (16) together with Eq. (18), one can obtain a surprisingly concise expression for the dispersion relation of wave motion in the sagittal plane

$$\cos(\kappa_3 a_3) = \frac{1}{4}\left[g_3(\omega,\kappa_1) \pm \sqrt{[g_3(\omega,\kappa_1)]^2 - 4g_2(\omega,\kappa_1) + 8}\right] \tag{19}$$

By exploring κ_1 within the range of [0, ∞), the complete picture of dispersion relation for sagittal plane waves can be determined over the κ_1–κ_3 plane. This newly derived analytical expression is adopted to study spectral distortions observed in the FE analysis of waves perpendicular to the layers in layered composites.

2.2 Wave Propagation Perpendicular to Composite Layers.

For the infinitely periodic layered composites, many researchers investigated the analytical dispersion relation of wave motion perpendicular to the layers [9,12,14,16,17]. This section will revisit its formulation by setting $\kappa_1 = 0$ in the procedure presented in Sec. 2.1.

For wave propagation perpendicular to the jth layer within the nth unit cell, we can easily obtain the displacement components by setting $\kappa_1 = 0$ in Eq. (6)

$$\begin{aligned} u_{3,j,n}(x_{3,j,n},t) &= \left[P_{F,j,n}\,e^{-i\omega x_{3,j,n}/c_{p,j}} + P_{B,j,n}\,e^{i\omega x_{3,j,n}/c_{p,j}}\right]e^{-i\omega t} \\ u_{1,j,n}(x_{3,j,n},t) &= \left[Q_{F,j,n}\,e^{-i\omega x_{3,j,n}/c_{s,j}} + Q_{B,j,n}\,e^{i\omega x_{3,j,n}c_{s,j}}\right]e^{-i\omega t} \end{aligned} \tag{20}$$

Similarly, the corresponding stresses of the jth layer in nth unit cell can be also obtained from Eq. (7)

$$\begin{aligned} \sigma_{33,j,n}(x_1,x_{3,j,n},t) &= \left[-P_{F,j,n}\omega\rho_j c_{p,j}e^{-\frac{i\omega d_j}{c_{p,j}}} + P_{B,j,n}\omega\rho_j c_{p,j}e^{\frac{i\omega d_j}{c_{p,j}}}\right]e^{-i\omega t} \\ \sigma_{31,j,n}(x_1,x_{3,j,n},t) &= \left[-Q_{F,j,n}\omega\rho_j c_{s,j}e^{-\frac{i\omega d_j}{c_{s,j}}} + Q_{B,j,n}\omega\rho_j c_{s,j}e^{\frac{i\omega d_j}{c_{s,j}}}\right]e^{-i\omega t} \end{aligned} \tag{21}$$

Four unknown coefficients, $P_{F,j,n}$, $P_{B,j,n}$, $Q_{F,j,n}$, and $Q_{B,j,n}$, can be determined from two displacement and two stress continuous

boundary conditions at the layer interface between the jth and the $(j+1)$th layers in the nth unit cell

$$[u_{3,j,n}]_{x_{3,j,n}=d_j} = [u_{3,j+1,n}]_{x_{3,j+1,n}=0}, \quad [u_{1,j,n}]_{x_{3,j,n}=d_j} = [u_{1,j+1,n}]_{x_{3,j+1,n}=0}$$
$$[\sigma_{33,j,n}]_{x_{3,j,n}=d_j} = [\sigma_{33,j,n}]_{x_{3,j+1,n}=0}, \quad [\sigma_{31,j,n}]_{x_{3,j,n}=d_j} = [\sigma_{31,j,n}]_{x_{3,j+1,n}=0} \tag{22}$$

After the application of Eq. (22) at all the interfaces, one can simultaneously obtain two decoupled sets of equations: one for pressure waves and the other for shear waves. Since the obtained two sets of equations are analogous, only the set of equations for pressure waves are considered in this section.

For pressure waves perpendicular to the layers, the successive applications of the boundary conditions from one interface to another eventually provide the following relation between the first layer of the nth unit cell and that of the $(n+1)$th unit cell:

$$\mathbf{W}_{p,1,n+1} = \mathbf{T}_p \mathbf{W}_{p,1,n} \tag{23}$$

where

$$\mathbf{W}_{p,1,n} = \begin{bmatrix} P_{F,1,n} \\ P_{B,1,n} \end{bmatrix}, \quad \mathbf{W}_{p,1,n+1} = \begin{bmatrix} P_{F,1,n+1} \\ P_{B,1,n+1} \end{bmatrix} \tag{24}$$

$$\begin{aligned} \mathbf{T}_p &= \mathbf{R}_{p,1}^{-1}(\mathbf{R}_{p,M}\mathbf{D}_{p,M}\mathbf{R}_{p,M}^{-1})\ldots(\mathbf{R}_{p,2}\mathbf{D}_{p,2}\mathbf{R}_{p,2}^{-1})\mathbf{R}_{p,1}\mathbf{D}_{p,1} \\ &= \mathbf{R}_{p,1}^{-1}\left(\prod_{j=2}^{M}\mathbf{R}_{p,M+2-j}\mathbf{D}_{p,M+2-j}\mathbf{R}_{p,M+2-j}^{-1}\right)\mathbf{R}_{p,1}\mathbf{D}_{p,1} \end{aligned} \tag{25}$$

$$\mathbf{R}_{p,j} = \begin{bmatrix} 1 & 1 \\ -\omega\rho_j c_{p,j} & \omega\rho_j c_{p,j} \end{bmatrix}, \quad \mathbf{D}_{p,j} = \begin{bmatrix} e^{-\frac{i\omega d_j}{c_{p,j}}} & 0 \\ 0 & e^{\frac{i\omega d_j}{c_{p,j}}} \end{bmatrix} \tag{26}$$

where the subscript p stands for pressure waves, and $\mathbf{T}_p$ is the transfer matrix which determines the relation between the amplitude vectors ($\mathbf{W}_{p,1,n}$ and $\mathbf{W}_{p,1,n+1}$) of adjacent unit cells.

In addition to the continuous boundary conditions, the application of the Bloch-periodic boundary condition provides another relation between adjacent unit cells

$$\mathbf{W}_{p,1,n+1} = e^{i\kappa_3 a_3}\mathbf{W}_{p,1,n} \tag{27}$$

After combining Eqs. (23) and (27), one can obtain an eigenvalue problem for pressure wave motion

$$\mathbf{T}_p\mathbf{W}_{p,n} = e^{i\kappa_3 a_3}\mathbf{W}_{p,n} \tag{28}$$

where $e^{i\kappa_3 a_3}$ and $\mathbf{W}_{p,1,n}$ are the eigenvalue and eigenvector of $\mathbf{T}_p$, respectively. By setting $\lambda = e^{i\kappa_3 a_3}$ as in Sec. 2.1, the characteristic polynomial equation of $\mathbf{T}_p$ can be written as

$$\lambda^2 - h_1\lambda + h_0 = 0 \tag{29}$$

with

$$h_1(\omega) = \mathrm{tr}(\mathbf{T}_p), \quad h_0(\omega) = \det(\mathbf{T}_p) \tag{30}$$

Analogous to the argument presented in Sec. 2.1, the reciprocal relation is found in the eigenvalues, i.e., $\lambda_2 = 1/\lambda_1$, resulting in

$$h_0(\omega) = 1 \tag{31}$$

Now, by solving the simplified characteristic polynomial equation (29) with Eq. (31), one can obtain a concise, closed-form solution of the dispersion relation for pressure wave propagation perpendicular to the layers

$$\cos(\kappa_3 a_3) = \frac{1}{2}h_1(\omega) = \frac{1}{2}\mathrm{tr}(\mathbf{T}_p) \tag{32}$$

For the infinitely periodic bilayered composites ($M=2$), the present analytical solution (32) recovers the well-known expression for the dispersion relation for waves perpendicular to the layers

$$\begin{aligned} \cos(a_3\kappa_3) = &\cos\left(\frac{\omega d_1}{c_{p,1}}\right)\cos\left(\frac{\omega d_2}{c_{p,2}}\right) \\ &-\frac{1}{2}\left(\frac{\rho_1 c_{p,1}}{\rho_2 c_{p,2}} + \frac{\rho_2 c_{p,2}}{\rho_1 c_{p,2}}\right)\sin\left(\frac{\omega d_1}{c_{p,1}}\right)\sin\left(\frac{\omega d_2}{c_{p,2}}\right) \end{aligned} \tag{33}$$

Similarly, the dispersion relation of shear wave propagation perpendicular to the layers can be also obtained by solving another decoupled eigenvalue problem, where the pressure wave-related quantities are simply replaced by the corresponding shear wave-related ones.

3 Numerical Dispersion Relations for Multilayered Periodic Composites

In this section, an issue with spatial discretization is presented to explain the spectral distortion in FE dispersion relations of infinitely periodic multilayered composites. For the sake of competentness of this article, we briefly review the discrete Fourier transform (DFT) although it is already summarized in our previous study [46].

3.1 Discrete Fourier Transform. We consider an unknown continuous spatial function $\chi(\mathbf{x})$ defined in the 2D coordinate space, and assume that only regularly spaced $N_1 \times N_3$ data for the unknown function $\chi(\mathbf{x})$ are available in a sampled region $x_1 \in [0, (N_1-1)\Delta x_1]$ and $x_3 \in [0, (N_3-1)\Delta x_3]$. Here, the discrete series of the data are represented by $\{\chi[p_1, p_3]\}$, where $p_k = 0, 1, 2, \ldots, N_k - 1$ for $k = 1, 3$. Now, the Fourier coefficients $\hat{\chi}_{\mathbf{g}}$ of the unknown continuous function $\chi(\mathbf{x})$ can be estimated as follows [52]:

$$\hat{\chi}_{\mathbf{g}} \approx \hat{\chi}[q_1, q_3] = \frac{1}{N_1 N_3}\sum_{p_1=0}^{N_1-1}\sum_{p_3=0}^{N_3-1}\chi[p_1, p_3]e^{-i2\pi\left(\frac{p_1 q_1}{N_1} + \frac{p_3 q_3}{N_3}\right)} \tag{34}$$

where the hat $\hat{\square}$ indicates quantities in the wavevector domain and $q_k = 0, 1, 2, \ldots, N_k - 1$ for $k = 1, 3$. Here, $\hat{\chi}[q_1, q_3]$ is referred as the DFT of the discrete series $\{\chi[p_1, p_3]\}$. In addition, there is an inverse formula by which a specific value of $\chi[p_1, p_3]$ in the space domain can be returned from the discrete series $\{\hat{\chi}[q_1, q_3]\}$ in the wavevector domain

$$\chi[p_1, p_3] = \sum_{q_1=0}^{N_1-1}\sum_{q_3=0}^{N_3-1}\hat{\chi}[q_1, q_3]e^{i2\pi\left(\frac{p_1 q_1}{N_1} + \frac{p_3 q_3}{N_3}\right)} \tag{35}$$

By the definition of DFT (34), the regularly spaced discrete spatial data $\chi[p_1, p_3]$ in the coordinate space engender the periodicity of the DFT coefficients

$$\hat{\chi}[q_1 + l_1 N_1, q_3 + l_3 N_3] = \hat{\chi}[q_1, q_3] \tag{36}$$

where l_1 and l_3 are arbitrary integers. The coefficients $\hat{\chi}[q_1, q_3]$ just repeat themselves for wavevector domain beyond $\kappa_1 \in [0, 2\pi/\Delta x_1]$ and $\kappa_3 \in [0, 2\pi/\Delta x_3]$. Furthermore, for a real-valued function $\chi(\mathbf{x})$, its DFT coefficients become conjugate symmetric with respect to the origin

$$\hat{\chi}[-q_1, -q_3] = \hat{\chi}^*[q_1, q_3] \tag{37}$$

where $\square^*$ indicates the complex conjugate. Therefore, the magnitude of the DFT coefficients $|\hat{\chi}[q_1, q_3]|$ is now symmetric around

multiples of $\pi/\Delta x_1$ and $\pi/\Delta x_3$ in the κ_1- and κ_3-axes, respectively. This symmetry is commonly referred as the zone folding [53], and the folding wavenumbers $\kappa_{1,f}$ and $\kappa_{3,f}$ are defined as

$$\kappa_{1,f} = \frac{\pi}{\Delta x_1}, \quad \kappa_{3,f} = \frac{\pi}{\Delta x_3} \tag{38}$$

Consequently, the calculated DFT coefficients are the only correct Fourier coefficient estimates for the wavevector domain enclosed by $\kappa_1 \in [0, \kappa_{1,f}]$ and $\kappa_3 \in [0, \kappa_{3,f}]$. This periodicity of the DFT entails infinitely many aliases of the true spectrum in the wavevector domain.

3.2 Spatial Aliasing. Assume that the unknown spatial function $\chi(\mathbf{x})$ in Sec. 3.1 contains wavenumber components beyond the wavevector domain of $\kappa_1 \in [0, \pi/\Delta x_1]$ and $\kappa_3 \in [0, \pi/\Delta x_3]$. Then, these high-wavenumber components falsely contribute to the DFT coefficient series calculated from the discretely measured data $\{\chi[p_1, p_3]\}$. This numerical issue is referred as spatial aliasing [52], and it can be alleviated by increasing the discrete sampling rate which enables to capture high-wavenumber components existing in the continuous function.

For infinitely periodic bilayered composites, we recently showed that spatial aliasing is the origin of fictitious modes observed in dispersion relation obtained in the FE framework [46]. In this paper, we extend our finding to infinitely periodic multilayered composites. In order to calculate the phononic dispersion relation of an infinitely periodic multilayered composite in the FE framework, a rectangular unit cell of $a_1 \times a_3$ has to be employed (see Fig. 1(*a*)) with periodic boundary condition along x_1 and x_3-axes. Note that the properties of the layered composite are a_3-periodic in the x_3-axis (i.e., the direction perpendicular to the layers shown in Fig. 1(*a*)) while they are continuous along the x_1-axis (i.e., the direction parallel to the layers shown in Fig. 1(*a*)). The wave characteristics of the multilayered composite relating to a_3-periodicity can be properly captured by using a unit cell length of $\Delta x_3 = a_3$ in the direction perpendicular to the layers. However, κ_1 components relating to homogeneous properties in x_1-direction cannot be fully accessed by using a unit cell length of $\Delta x_1 = a_1$ in the direction parallel to the layers. To make things worse, even an artificial $2\pi/a_1$-periodicity occurs along the κ_1-axis due to the use of a finite size unit cell in x_1-axis. For infinitely periodic multilayered composites, Sec. 4 illustrates that aliasing-induced spectral distortions occur due to the inevitable use of a finite size unit cell in the FE framework.

4 Comparison and Analysis

Regarding the dispersion relations of infinitely periodic layered composites, the analytical [9–14] and the numerical [34,35,37] studies in the literature predominantly investigate only bilayered composites. Note that the FE method is an efficient tool to numerically calculate the dispersion relations of any periodic structures, but it entails fictitious modes in layered composites regardless of the number of layers. Section 2 in this article clearly shows that analytical dispersion relations of infinitely periodic layered composites can be obtained for any number of layers. Thus, to highlight spectral distortions in the FE framework, we present the dispersion relations of two specific infinitely periodic multilayered composites, which contain more periodic layers than bilayer composites.

4.1 Geometry, Materials, and Numerical Model. Two different infinitely periodic multilayered composites are selected to investigate the origin of the spectral distortions observed in FE dispersion relations: one with an infinitely periodic three-layered composite and the other with an infinitely periodic four-layered one. Basically, these two composite cases are provided to show that the spatial aliasing solution presented in this study is applicable to any infinitely periodic multilayered composites regardless of the number of periodic layers. The unit cell of the infinitely periodic three-layered composite consists of steel ($d_1 = 0.4$ mm), aluminum ($d_2 = 0.4$ mm), and copper ($d_3 = 0.2$ mm), so the periodic length of the composite in the x_3-axis is $a_3 = \sum_{j=1}^{3} d_j = 1$ mm. On the other hand, for the infinitely periodic four-layered composite, the unit cell is composed of steel ($d_1 = 0.4$ mm), aluminum ($d_2 = 0.2$ mm), copper ($d_3 = 0.2$ mm), and titanium ($d_4 = 0.2$ mm), resulting in the periodic length of $a_3 = 1$ mm. The properties of the considered materials are listed in Table 1.

As discussed in Sec. 3.2, the numerical procedure for dispersion analysis in the FE framework requires the use of a rectangular unit cell in the 2D coordinate space. In order to highlight the effect of the aspect ratio of a_1/a_3 in the considered unit cell, we use two different aspect ratios $a_1/a_3 = 2.0$, and $a_1/a_3 = 1.0$ for the both composites. Figures 2(*a*) and 3(*a*) describe the geometries and the corresponding Brillouin/aliasing zones of the infinitely periodic three-layered composite models with $a_1/a_3 = 2.0$ and $a_1/a_3 = 1.0$, respectively. The analogous schematic diagrams for the infinitely periodic four-layered models with $a_1/a_3 = 2.0$ and $a_1/a_3 = 1.0$ are also shown in Figs. 4(*a*) and 5(*a*), respectively.

Plane strain conditions are assumed in all the FE simulations, so all the 2D FE models are constructed using four-node bilinear plane strain elements (CPE4R elements in ABAQUS). The detailed procedure to obtain dispersion relation using the FE method can be found in Refs. [42] and [46]. Through a mesh refinement study, we select the mesh size of $0.025a_3$ to ensure the convergence of the FE simulations.

4.2 Numerical Dispersion Relations in the Finite Element Framework. In order to obtain the dispersion relations of infinitely periodic multilayered composites, researchers in the FE community have arbitrarily selected a thin unit cell without a clear understanding of the routine [34,35,37]. Specific examples in this section will show that FE dispersion relations should be carefully interpreted because their results contain undesired fictitious modes and show strong dependence on the configuration of the employed unit cell.

For the infinitely periodic three-layered composite, Figs. 2(*b*) and 3(*b*) illustrate the numerical dispersion relations obtained using the FE models with the aspect ratios of $a_1/a_3 = 2.0$ and $a_1/a_3 = 1.0$, respectively. Those two figures show two types of lines. The first type is the set of (blue) solid lines with dot markers representing the correct dispersion relation for waves propagation perpendicular to the layers, and the second type is the set of the (red) solid lines corresponding fictitious modes. In the FE framework, those two types of modes are obtained simultaneously and they cannot be separated. We separate those two types of modes by comparing FE results with the analytical solution, which will be discussed in Sec. 4.3. From the FE model with the aspect ratio of $a_1/a_3 = 2.0$, the first fictitious mode appears around the normalized frequency of $\bar{\omega} = \omega a_3/(2\pi c_{s,2}) = 0.5$. On the other hand, the FE model with $a_1/a_3 = 1.0$ produces the first fictitious modes around $\bar{\omega} = 1.0$. As the aspect ratio of the unit cell (i.e., a_1/a_3) increases, the first fictitious mode tends to emerge at lower frequencies. For the infinitely periodic four-layered composite, a similar trend is also observed in the numerical dispersion relations for wave propagation perpendicular to the layers. In Figs. 4(*b*) and 5(*b*), the first fictitious mode is observed around $\bar{\omega} = 0.5$ and $\bar{\omega} = 1.0$ from the FE model with $a_1/a_3 = 2.0$ and $a_1/a_3 = 1.0$, respectively. Note that any aspect ratio (even smaller than 1.0) can also be explored, but the FE dispersion relations will contain fictitious

Table 1 Properties of considered materials

Index, j	Material	ρ (kg/m^3)	λ (GPa)	μ (GPa)
1	Steel	7800	121.2	80.8
2	Aluminum	2700	51.1	26.3
3	Copper	8960	95.1	47.7
4	Titanium	4500	78.1	43.9

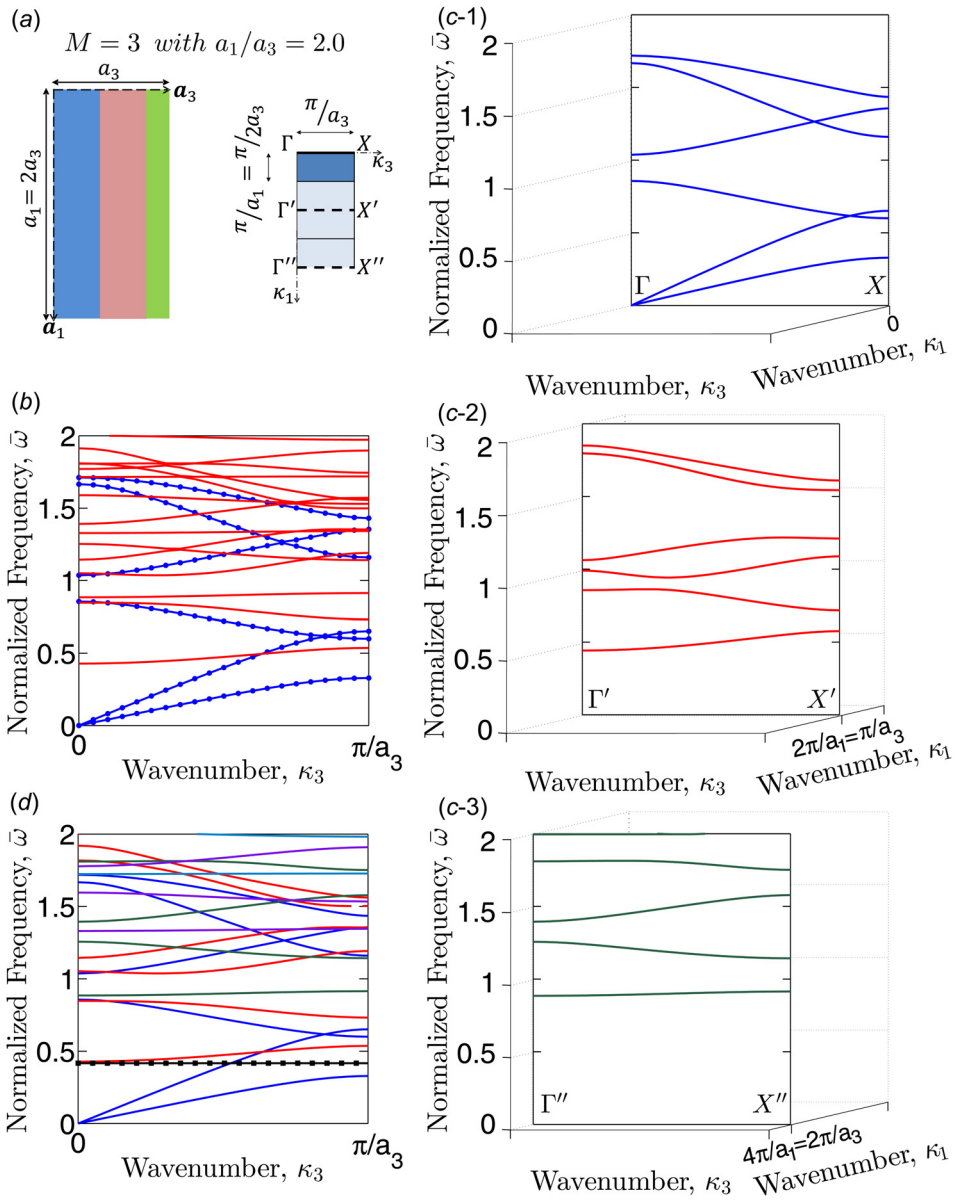

Fig. 2 (*a*) (Left) A unit cell of the infinitely periodic three-layered composite having $a_1/a_3 = 2.0$, which is employed for numerical dispersion analysis. (Right) The corresponding wavevector domain, which illustrates the valid wavevector path for waves perpendicular to the layers (Γ–X) and the corresponding aliasing paths (Γ'–X', Γ''–X''). (*b*) FE dispersion relation obtained by employing a unit cell of $a_1/a_3 = 2.0$. Note that the numerical dispersion relation contains unwanted fictitious modes represented by red solid lines. (*c*) Three analytical dispersion relations obtained from Eq. (19): (*c*-1) $\kappa_1 = 0$, (*c*-2) $\kappa_1 = 2\pi/a_1$, and (*c*-3) $\kappa_1 = 4\pi/a_1$. (*d*) The projection of all the analytical dispersion relations in Fig. 2(*c*) onto the $\kappa_3 - \omega$ plane. Note that one can find one-to-one map in all the observed wave modes in Figs. 2(*b*) and 2(*d*), indicating that the fictitious modes originate from the aliasing paths. Moreover, the maximum valid frequency ω_{max} from Eq. (44) is denoted by a line with square markers.

modes regardless of the magnitude of the aspect ratio (e.g., see Ref. [46]). The two aspect ratios (i.e., $a_1/a_3 = 2.0$, 1.0) in this study are merely chosen to efficiently demonstrate the effect of the aspect ratio on the appearance of fictitious modes.

4.3 Analytical Dispersion Relation and Spatial Aliasing. Using the analytical solution of sagittal plane waves (19), the dispersion relations of infinitely periodic multilayered composites can be calculated along specific wavevector paths. Due to the homogeneous properties along x_1-direction, wave motion in the infinitely periodic multilayered composites contains infinitely large κ_1 components. For the infinitely periodic three-layered composite, the sagittal plane wave solution (19) shows the non-periodic characteristics of true dispersion relation in the direction parallel to the layers (see Fig. 6(*a*-1) with $\kappa_3 = 0$ and Fig. 6(*a*-2) with $\kappa_3 = \pi/a_3$). Figures 6(*b*-1) and 6(*b*-2) also show a similar trend for the infinitely periodic four-layered composite. However, the spatial discretization by using a rectangular unit cell of $a_1 \times a_3$ in the FE framework induces the artificial $2\pi/a_1$-periodicity in the κ_1-axis of the wavevector domain as discussed in Sec. 3.2. Furthermore, it entails an infinitely many aliases of the true phononic

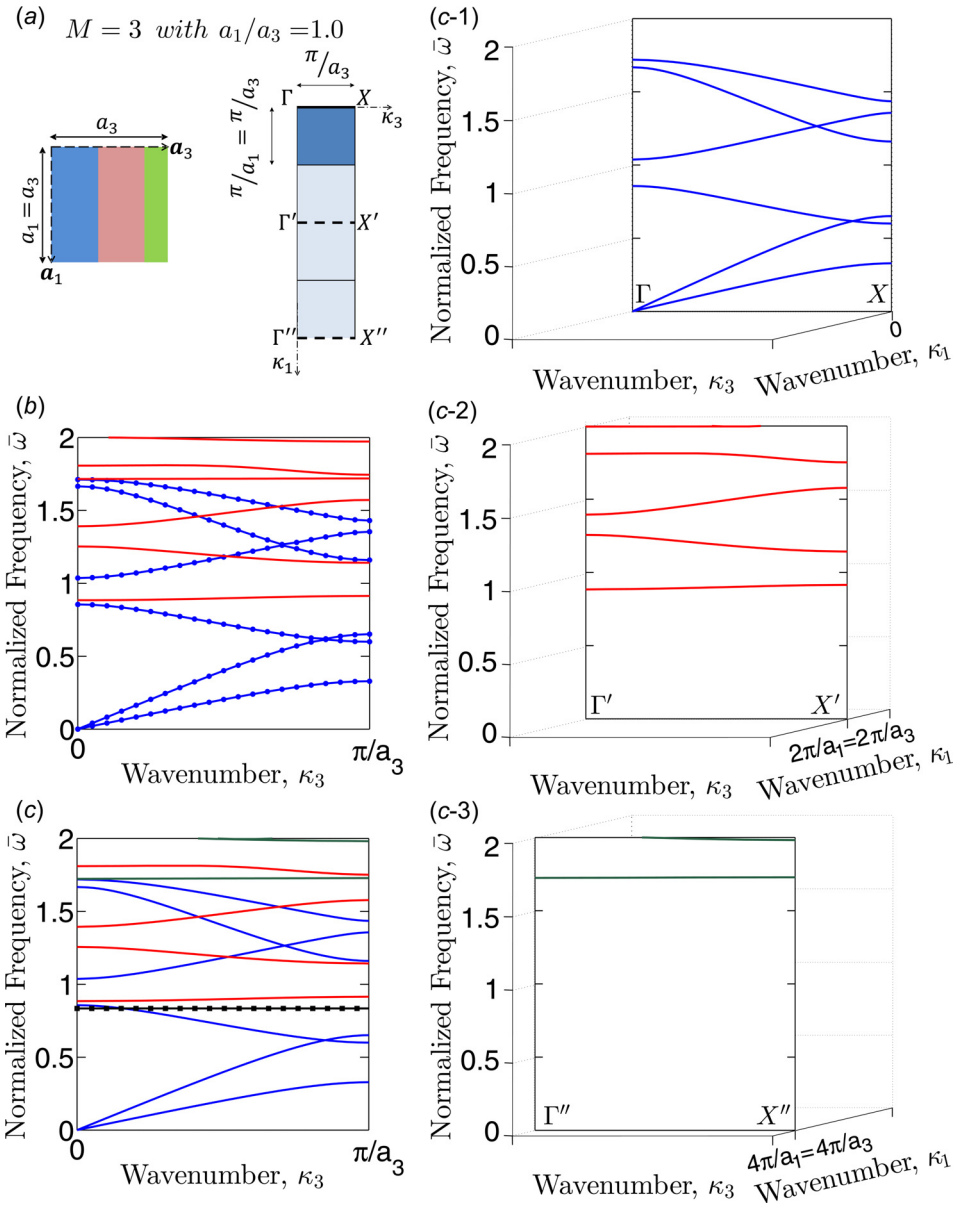

Fig. 3 (*a*) (Left) A unit cell of the infinitely periodic three-layered composite having $a_1/a_3 = 1.0$, which is employed for numerical dispersion analysis. (Right) The corresponding wavevector domain, which illustrates the valid wavevector path for waves perpendicular to the layers (Γ–X) and the corresponding aliasing paths ($\Gamma'-X'$, $\Gamma''-X''$). (*b*) FE dispersion relation obtained by employing a unit cell of $a_1/a_3 = 1.0$. Note that the numerical dispersion relation contains unwanted fictitious modes represented by red solid lines. (*c*) Three analytical dispersion relations obtained from Eq. (19): (*c*-1) $\kappa_1 = 0$, (*c*-2) $\kappa_1 = 2\pi/a_1$, and (*c*-3) $\kappa_1 = 4\pi/a_1$. (*d*) The projection of all the analytical dispersion relations in Fig. 3(*c*) onto the $\kappa_3 - \omega$ plane. Note that one can find one-to-one map in all the observed wave modes in Figs. 3(*b*) and 3(*d*), indicating that the fictitious modes originate from the aliasing paths. Moreover, the maximum valid frequency ω_{max} from Eq. (44) is denoted by a line with square markers.

dispersion relation, causing spectral distortions in numerical dispersion relation. In the following, the sagittal plane wave solution (19) is adopted to reproduce the distorted dispersion relations shown in Sec. 4.2.

The infinitely periodic three-layered composites are first considered. Recall that Fig. 2(*b*) shows the FE dispersion relation obtained by using a unit cell having $a_1/a_3 = 2.0$. Using the sagittal wave solution (19), we obtain the analytical dispersion relations at three different κ_1 values, all of which are multiples of $2\kappa_{1,f} = 2\pi/a_1$. In other words, the analytical dispersion relation with $\kappa_1 = 0$ (i.e., the path Γ–X in Fig. 2(*a*)) is shown in Fig. 2(*c*-1), and it represents the dispersion relation for waves perpendicular to the layers. In addition, Figs. 2(*c*-2) and 2(*c*-3) illustrate the sagittal wave solution (19) at $\kappa_1 = 2\kappa_{1,f}$ (i.e., $\Gamma' - X'$) and $\kappa_1 = 4\kappa_{1,f}$ (i.e., $\Gamma'' - X''$), respectively. Then, all the analytical dispersion relations calculated at different κ_1 values ($\kappa_1 = 0$, $2\kappa_{1,f}$, $4\kappa_{1,f}$, $6\kappa_{1,f}$, etc.) are projected onto the $\kappa_3 - \omega$ plane, and the projected dispersion relation is shown in Fig. 2(*d*). By comparing Figs. 2(*b*) and 2(*d*), one can find one-to-one correspondence in all the observed wave modes. Thus, the comparison between Figs. 2(*b*) and 2(*d*) shows that spectral distortions in the FE dispersion relations are induced by spacial aliasing originated from $\Gamma' - X'$, $\Gamma'' - X''$, etc., which are the aliasing paths of $\Gamma - X$ in the first Brillouin zone. Similarly, in Fig. 3, the numerical dispersion relation

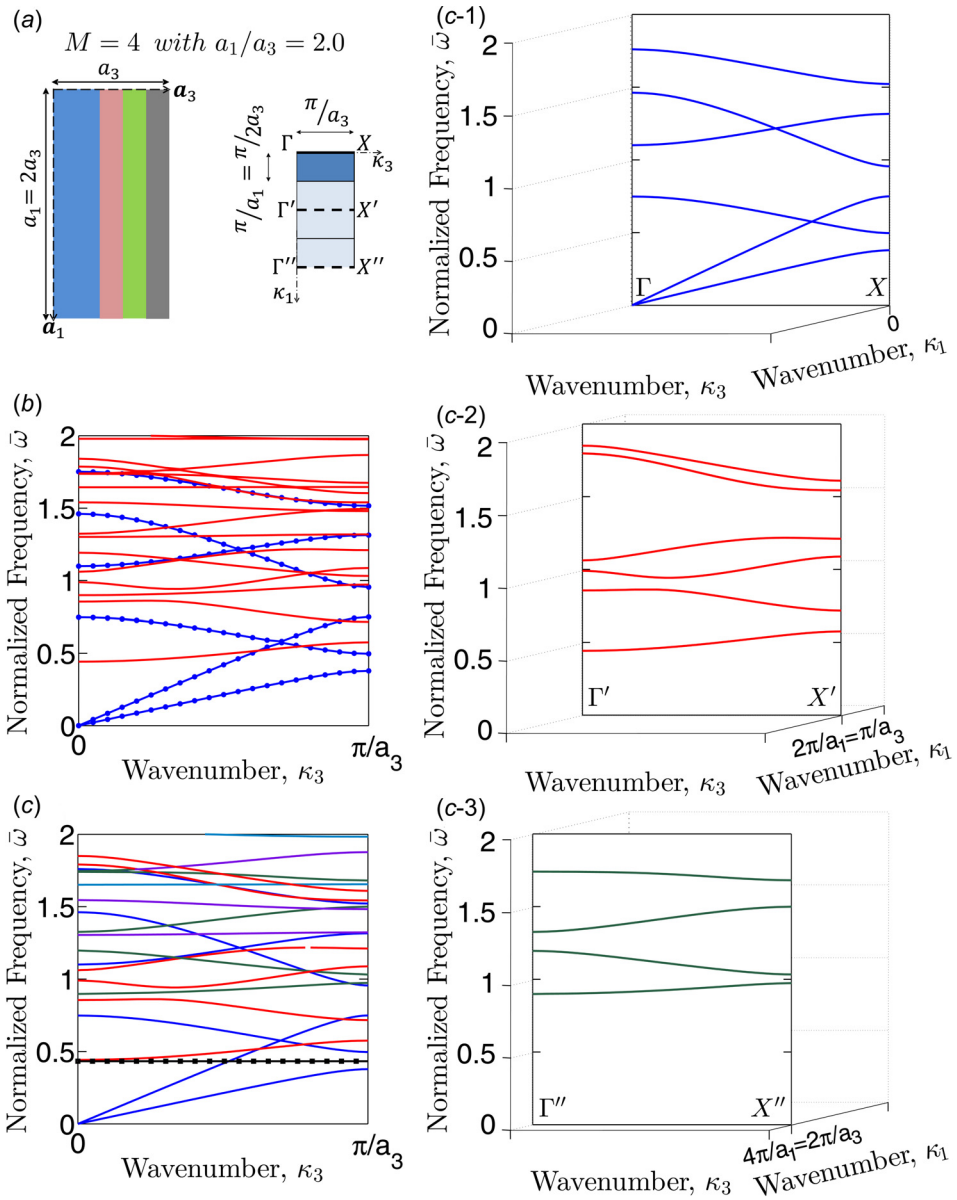

Fig. 4 (*a*) (Left) A unit cell of the infinitely periodic four-layered composite having $a_1/a_3 = 2.0$, which is employed for numerical dispersion analysis. (Right) The corresponding wavevector domain, which illustrates the valid wavevector path for waves perpendicular to the layers (Γ – *X*) and the corresponding aliasing paths ($\Gamma'-X'$, $\Gamma''-X''$). (*b*) FE dispersion relation obtained by employing a unit cell of $a_1/a_3 = 2.0$. Note that the numerical dispersion relation contains unwanted fictitious modes represented by red solid lines. (*c*) Three analytical dispersion relations obtained from Eq. (19): (*c*-1) $\kappa_1 = 0$, (*c*-2) $\kappa_1 = 2\pi/a_1$, and (*c*-3) $\kappa_1 = 4\pi/a_1$. (*d*) The projection of all the analytical dispersion relations in Fig. 4(*c*) onto the $\kappa_3 - \omega$ plane. Note that one can find one-to-one map in all the observed wave modes in Figs. 4(*b*) and 4(*d*), indicating that the fictitious modes originate from the aliasing paths. Moreover, the maximum valid frequency ω_{max} from Eq. (44) is denoted by a line with square markers.

obtained from the FE model with a unit cell having the aspect ratio of $a_1/a_3 = 1.0$ (i.e., Fig. 3(*b*)) are compared with the analytical dispersion relations obtained from sagittal plane waves (i.e., Fig. 3(*d*)). Furthermore, for the infinitely periodic four-layered composites, Figs. 4 and 5 compare the sagittal plane wave dispersion relations with the numerical result obtained from the FE models having the aspect ratios of $a_1/a_3 = 2.0$ and 1.0, respectively.

The results presented in Figs. 2–5 clearly show that a smaller aspect ratio in FE modeling introduces fictitious modes at higher frequencies, thus resulting in fewer fictitious modes in the presented graphs. The sagittal plane wave solutions prove that the fictitious modes occur at the aliasing paths. In the wavenumber domain, the distance of the aliasing paths (i.e., $\Gamma' - X'$, $\Gamma'' - X''$, etc.) from the wavevector path Γ–X within the first Brillouin zone can be expressed by

$$\kappa_{1,l} = \frac{2\pi l}{a_1} \tag{39}$$

where l is an integer. Thus, as the aspect ratio decreases (i.e., a_1 decreases), $\kappa_{1,l}$ increases (see Fig. 1(*b*)). Consequently, due to the proportional relation between wavenumber and the corresponding

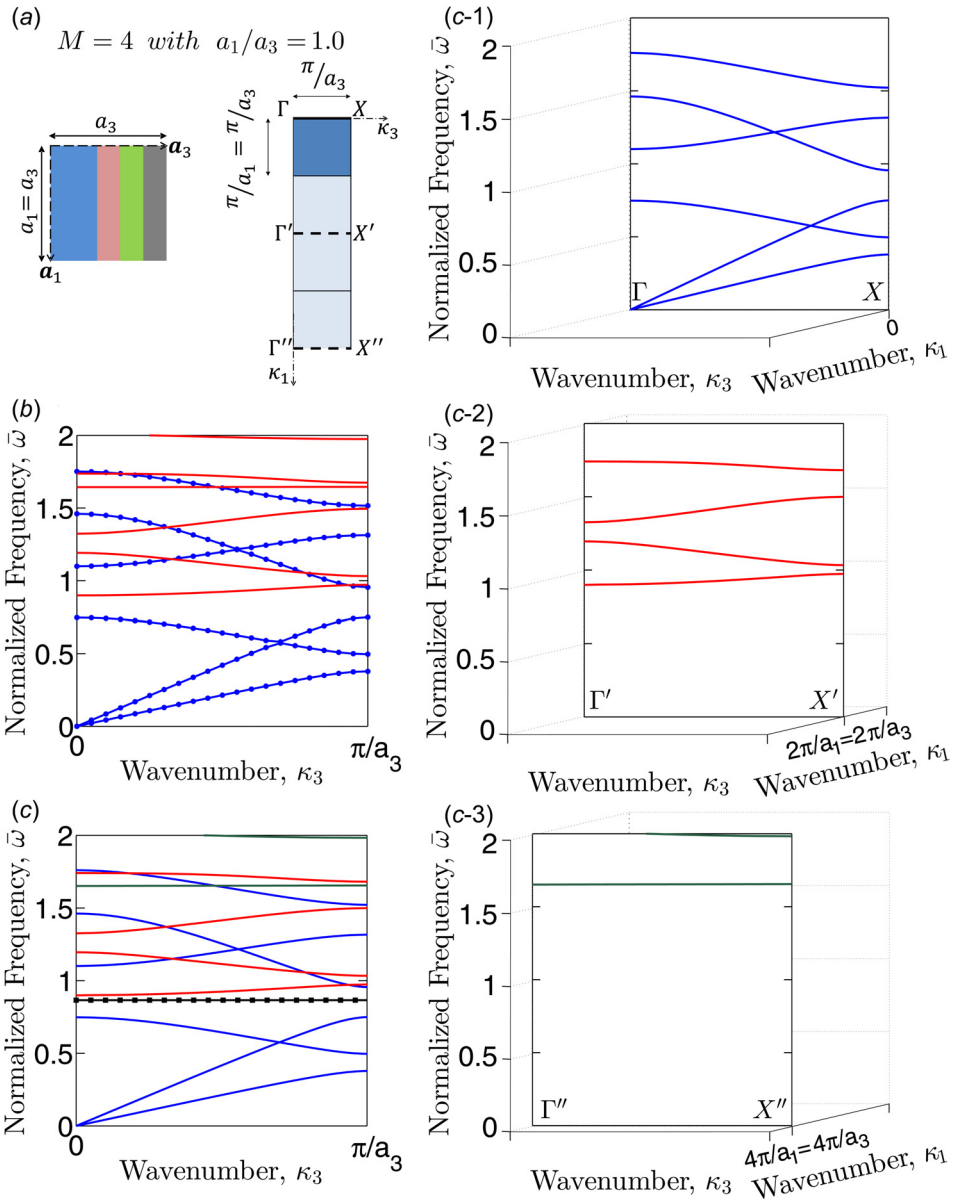

Fig. 5 (*a*) (Left) A unit cell of the infinitely periodic four-layered composite having $a_1/a_3 = 1.0$, which is employed for numerical dispersion analysis. (Right) The corresponding wavevector domain, which illustrates the valid wavevector path for waves perpendicular to the layers (Γ–X) and the corresponding aliasing paths ($\Gamma'-X'$, $\Gamma''-X''$). (*b*) FE dispersion relation obtained by employing a unit cell of $a_1/a_3 = 1.0$. Note that the numerical dispersion relation contains unwanted fictitious modes represented by red solid lines. (*c*) Three analytical dispersion relation obtained from Eq. (19): (*c*-1) $\kappa_1 = 0$, (*c*-2) $\kappa_1 = 2\pi/a_1$, and (*c*-3) $\kappa_1 = 4\pi/a_1$. (*d*) The projection of all the analytical dispersion relations in Fig. 5(*c*) onto the $\kappa_3 - \omega$ plane. Note that one can find one-to-one map in all the observed modes in Figs. 5(*b*) and 5(*d*), indicating that the fictitious modes originate from the aliasing paths. Moreover, the maximum valid frequency ω_{max} from Eq. (44) is denoted by a line with square markers.

frequency in elastic wave motion, fictitious modes appear at higher frequencies as a_1 decreases.

In summary, aliasing-induced spectral distortions in FE dispersion relations are reproduced through the newly derived sagittal plane wave solution for infinitely periodic multilayered composites (19).

5 Discussion on Finite Element Modeling Guideline for Indefinitely Periodic Multilayered Composites

For infinitely periodic *bilayered* composites, our previous study [46] suggested a FE modeling guideline, which determines a proper FE model configuration to obtain a valid numerical dispersion relation of waves perpendicular to the layers. In this section, we extend the derivation beyond infinitely periodic bilayered composites, and offer a generalized FE modeling guideline which can cover infinitely periodic *multilayered* composites. For the dispersion relation of infinitely periodic multilayered composites, fictitious modes occur at the several aliasing paths, i.e., multiples of $2\kappa_{1,f}$ in the κ_1-axis. Recall that $\kappa_{1,f}$ is the folding wavenumber, $\kappa_{1,f} = \pi/\Delta x_1 = \pi/a_1$. If a unit cell of $a_1 \times a_3$ is employed in the FE modeling of the layered composite shown in Fig. 1(*a*), the corresponding numerical dispersion relation is not impaired by the existence of the spatial aliasing up to $\kappa_1 = \kappa_{1,\max}$

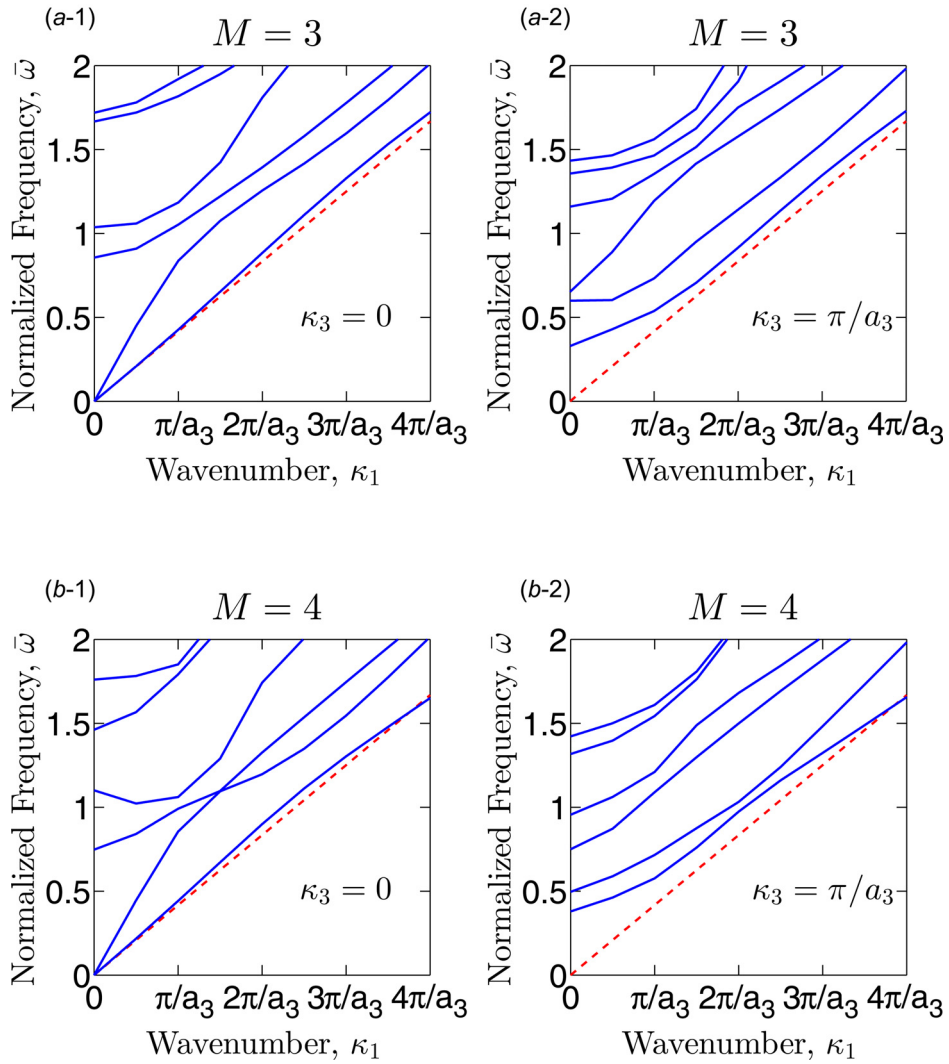

Fig. 6 (*a*) Analytical dispersion relation obtained from Eq. (19) for the infinitely periodic three-layered composite: (*a*-1) $\kappa_3 = 0$ and (*a*-2) $\kappa_3 = \pi/a_3$. (*b*) Analytical dispersion relation obtained from Eq. (19) for the infinitely periodic four-layered composite: (*b*-1) $\kappa_3 = 0$ and (*b*-2) $\kappa_3 = \pi/a_3$. The dotted lines denote the approximated linear dispersion relations obtained from the effective modulus theory (41). Note that the κ_1 axis is intentionally normalized by a_3 because the periodic length a_3 is the common characteristic length of the considered periodic composites.

$$\kappa_{1,\max} < 2\kappa_{1,f} = \frac{2\pi}{a_1} \quad \Longleftrightarrow \quad a_1 < \frac{2\pi}{\kappa_{1,\max}} \tag{40}$$

In other words, the second inequality of Eq. (40) indicates a proper unit cell size a_1 in the FE framework for a given wavenumber of interest, $\kappa_{1,\max}$. The above anti-aliasing condition is valid regardless of the number of layers per unit cell of infinitely periodic layered composites.

However, the number of layers per unit cell should be carefully considered in order to suggest a FE model guideline in terms of the frequency ω of propagating waves rather than the wavenumber κ_1. Note that numerical dispersion analysis of infinitely periodic multilayered composites is typically represented in the space of $\kappa_3 - \omega$ (refer Figs. 2(*b*), 3(*b*), 4(*b*), and 5(*b*)). In order to explore a relation between the wavenumber κ_1 and the frequency ω of propagation waves, we adopt the effective modulus theory for infinitely periodic multilayered composites [54]. As long as each layer's thickness is sufficiently small compared to the wavelength of a harmonic excitation, the effective modulus theory states that an infinitely periodic multilayered composite behaves as a transversely isotropic continuum [54]. In the direction parallel to the layers (i.e., x_1-direction in Fig. 1(*a*)), the effective modulus theory for infinitely periodic multilayered composites suggests an approximate linear relation between the wavenumber κ_1 and the frequency ω of waves for the lowest wave mode

$$\omega \simeq \frac{2\pi\bar{c}_s}{\lambda_1} = \bar{c}_s\kappa_1 \tag{41}$$

where the effective shear wave velocity $\bar{c}_s$ is employed because the lowest wave mode always comes from shear waves, not from pressure waves [10]. Here, for infinitely periodic multilayered composites, the wave velocity $\bar{c}_s$ is defined using the effective mass density $\bar{\rho}$ and the effective elastic constant $\bar{c}_{44}$ as

$$\bar{c}_s = \sqrt{\bar{c}_{44}/\bar{\rho}} \tag{42}$$

where

$$\bar{\rho} = \sum_{j=1}^{M} n_j\rho_j, \quad \frac{1}{\bar{c}_{44}} = \sum_{j=1}^{M}\frac{n_j}{\mu_j}, \quad n_j = \frac{d_j}{\sum_{k=1}^{M} d_k} \tag{43}$$

Here, the bar notation $\bar{\square}$ denotes the effective quantities of the infinitely periodic multilayered composites. For waves in the direction parallel to the layers (i.e., $\kappa_3 = 0$, π/a_3), Fig. 6 shows that the approximate linear frequency-wavenumber relation based on the effective modulus theory (41) (denoted by the dotted lines) is well compared with the lowest wave mode of the sagittal plane wave solution. Note that the linear relation between ω and κ given by Eq. (41) is limited to body waves (i.e., longitudinal and transverse wave motion) of infinitely periodic multilayerd composites which have infinite length in all directions. These relations cannot be applied to periodic plate structures which are characterized by the traction-free boundary conditions on top and bottom surfaces, because surface waves are typically the main interest. The studies on periodic plates using the FE framework [55–58] have shown that the dispersion relations of periodic plates are substantially different from the corresponding infinitely periodic phononic crystals. In addition, the wave finite element (WFE) method has been often adopted to investigate the dispersion relations of layered composite plates [59–63]. Some researchers reported an spatial aliasing issue in their analysis [59,60], and preformed a set of sensitivity study on the appearance of fictitious modes by changing the aspect ratio of their WFE unit cell. Although our guideline proposed to body waves of infinitely periodic multilayerd composites cannot be directly applicable to periodic plates, the finding and the procedure presented in this manuscript can be adopted to elegantly resolve the spatial aliasing issue reported in the dispersion relations of periodic plates.

By substituting the approximate linear relation (41) into the anti-aliasing condition (40), the following generalized FE modeling guideline is obtained:

$$a_1 < \frac{2\pi\,\bar{c}_s}{\omega_{\max}} \iff \omega_{\max} < \frac{2\pi\,\bar{c}_s}{a_1} = \frac{2\pi}{a_1}\left[\left(\sum_{j=1}^{M} n_j\rho_j\right)\left(\sum_{j=1}^{M}\frac{n_j}{\mu_j}\right)\right]^{-1/2} \tag{44}$$

Using Eq. (44), one can determine an adequate FE unit cell size a_1 of infinitely periodic multilayered composites for the highest frequency of interest ($\omega_{\max}$). The resultant equations in Eq. (44) consider the number of layers per unit cell of infinitely periodic multilayered composites, which affect the effective shear wave velocity $\bar{c}_s$ described in Eq. (42). In this regard, this study provides the generalized FE modeling guideline which is applicable to infinitely periodic multilayered composites. In Figs. 2(*d*), 3(*d*), 4(*d*), and 5(*d*), the maximum valid frequency $\omega_{\max}$ suggested from Eq. (44) are denoted by a black horizontal line with square markers for the considered unit cell size of a_1. Regardless of the number of layers and the unit cell configurations, no fictitious modes are observed below the maximum valid frequency $\omega_{\max}$ suggested from Eq. (44). Thus, the validity of the proposed guideline (44) is demonstrated, so that it can be applicable for numerical dispersion relations of general infinitely periodic multilayered composites.

6 Conclusion

The FE method offers an efficient framework to investigate the evolution of phononic crystals that possess materials or geometric nonlinearity subject to external loading. Despite its superior efficiency, the FE method suffers from spectral distortions in the dispersion analysis of infinitely periodic multilayered composites. Based on our recent study on spectral distortions in the FE dispersion relations of infinitely periodic *bilayered* composites [46], we extend our investigation to general infinitely periodic *multilayered* composites. We first rederive the analytical sagittal plane wave solution in a substantially concise form and reproduce aliasing-induced spectral distortions in FE dispersion using the derived analytical solution. Furthermore, combining an anti-aliasing condition and the effective elastic modulus theory, we provide a generalized FE modeling guideline to overcome the observed spectral distortions in FE dispersion relations of infinitely periodic multilayered composites. For a frequency range of interest, the suggested FE modeling guideline can be adopted to obtain a valid FE dispersion relation for wave propagation perpendicular to the layers of infinitely periodic multilayered composites. To be clear, our guideline cannot be applied to nonlinear wave motion such as amplitude-dependent wave dispersion relations because the effective modulus theory is employed. However, in order to study the evolution of dispersion relation of a periodic composite subject to external loading, the FE method typically adopts a two-step manner, i.e., nonlinear static analysis and then dispersion analysis. In the dispersion analysis step, the proposed FE modeling guideline is still applicable to a deformed periodic structure, which is the outcome from the nonlinear static analysis step. Thus, the proposed FE modeling guideline can be used for investigating the evolution of the band-structure of infinitely periodic multilayered composites.

Acknowledgment

This work has been partially supported by Qatar National Research Fund through Grant No. NPRP8-1568-2-666. Shim acknowledges start-up funds from the University at Buffalo (UB), and he is grateful to the support of UB Center for Computational Research.

References

[1] Saini, G., Pezeril, T., Torchinsky, D. H., Yoon, J., Kooi, S. E., Thomas, E. L., and Nelson, K. A., 2007, "Pulsed Laser Characterization of Multicomponent Polymer Acoustic and Mechanical Properties in the Sub-GHZ Regime," J. Mater. Res., **22**(3), pp. 719–723.
[2] Liang, B., Guo, X. S., Tu, J., Zhang, D., and Cheng, J. C., 2010, "An Acoustic Rectifier," Nat. Mater., **9**(12), pp. 989–992.
[3] Wang, Y., Song, W., Sun, E., Zhang, R., and Cao, W., 2014, "Tunable Passband in One-Dimensional Phononic Crystal Containing a Piezoelectric $0.62Pb(Mg_{1/3}Nb_{2/3})O_3$–$0.38PbTiO_3$ Single Crystal Defect Layer," Physica E, **60**, pp. 37–41.
[4] Cheng, W., Gomopoulos, N., Fytas, G., Gorishnyy, T., Walish, J., Thomas, E. L., Hiltner, A., and Baer, E., 2008, "Phonon Dispersion and Nanomechanical Properties of Periodic 1d Multilayer Polymer Films," Nano Lett., **8**(5), pp. 1423–1428.
[5] Nemat-Nasser, S., Sadeghia, H., Amirkhizib, A. V., and Srivastavac, A., 2015, "Phononic Layered Composites for Stress-Wave Attenuation," Mech. Res. Commun., **68**, pp. 65–69.
[6] Ma, C., Parker, R. G., and Yellen, B. B., 2013, "Optimization of an Acoustic Rectifier for Uni-Directional Wave Propagation in Periodic Mass-Spring Lattices," J. Sound Vib., **332**(20), pp. 4876–4894.
[7] Nemat-Nasser, S., and Srivastava, A., 2011, "Negative Effective Dynamic Mass-Density and Stiffness: Micro-Architecture and Phononic Transport in Periodic Composites," AIP Adv., **1**(4), p. 041502.
[8] Zhu, R., Huang, G. L., and Hu, G. K., 2012, "Effective Dynamic Properties and Multi-Resonant Design of Acoustic Metamaterials," ASME J. Vib. Acoust., **134**(3), p. 031006.
[9] Rytov, S. M., 1956, "Acoustical Properties of a Thinly Laminated Medium," Sov. Phys. Acoust., **2**(1), pp. 68–80.
[10] Sun, C. T., Achenbach, J. D., and Herrmann, G., 1968, "Time-Harmonic Waves in a Stratified Medium Propagating in the Direction of the Layering," ASME J. Appl. Mech., **35**(2), pp. 408–411.
[11] Achenbach, J. D., 1968, "Wave Propagation in Lamellar Composite Materials," J. Acoust. Soc. Am., **43**(6), pp. 1451–1452.
[12] Lee, E. H., and Yang, H. W., 1973, "On Waves in Composite Materials With Periodic Structure," Soc. Ind. Appl. Math., **25**(3), pp. 492–499.
[13] Brekhovskikh, L. M., 1980, "Waves in Layered Media," 2nd ed., *Applied Mathematics and Mechanics*, Vol. 16, Academic Press, New York.
[14] He, J. J., Djafarirouhani, B., and Sapriel, J., 1988, "Theory of Light Scattering by Longitudinal-Acoustic Phonons in Superlattices," Phys. Rev. B, **37**(8), pp. 4086–4098.
[15] Tamura, S., and Wolfe, J. P., 1988, "Acoustic Phonons in Multiconstituent Superlattices," Phys. Rev. B, **38**(8), pp. 5610–5614.
[16] Esquivel-Sirvent, R., and Cocoletzi, G. H., 1994, "Band Structure for the Propagation of Elastic Waves in Superlattices," J. Acoust. Soc. Am., **95**(1), pp. 86–90.
[17] Hussein, M. I., Hulbert, G. M., and Scott, R. A., 2006, "Dispersive Elastodynamics of 1d Banded Materials and Structures: Analysis," J. Sound Vib., **289**(4–5), pp. 779–806.
[18] Rouhani, B. D., Dobrzynski, L., Duparc, O., Camley, R., and Maradudin, A., 1983, "Sagittal Elastic Waves in Infinite and Semi-Infinite Superlattices," Phys. Rev. B, **28**(4), pp. 1711–1720.

[19] Nougaoui, A., and Rouhani, B. D., 1987, "Elastic Waves in Periodically Layered Infinite and Semi-Infinite Anisotropic Media," Surf. Sci., **185**(1–2), pp. 125–153.
[20] Nougaoui, A., and Rouhani, B. D., 1988, "Complex Band Structure of Acoustic Waves in Superlattices," Surf. Sci., **199**(3), pp. 623–637.
[21] Sapriel, J., and Rouhani, B. D., 1989, "Vibrations in Superlattices," Surf. Sci. Rep., **10**(4–5), pp. 189–275.
[22] Nayfeh, A. H., 1991, "The General Problem of Elastic Wave Propagation in Multilayered Anisotropic Media," J. Acoust. Soc. Am., **89**(4), pp. 1521–1531.
[23] Braga, A. M. B., and Herrmann, G., 1992, "Floquet Waves in Anisotropic Periodically Layered Composites," J. Acoust. Soc. Am., **91**(3), pp. 1211–1227.
[24] Hegemier, G. A., and Nayfeh, A. H., 1973, "A Continuum Theory for Wave Propagation in Laminated Composites—Case 1: Propagation Normal to Laminates," ASME J. Appl. Mech., **40**(2), pp. 503–510.
[25] Hegemier, G. A., and Bache, T. C., 1974, "A General Continuum Theory With Microstructure for Wave Propagation in Elastic Laminated Composites," ASME J. Appl. Mech., **41**(1), pp. 101–105.
[26] Herrmann, G., and Achenbach, J., 1967, "On Dynamic Theories of Fiber-Reinforced Composites," Eighth Structural Dynamics and Materials Conference, Palm Springs, CA, Mar. 29–31, pp. 112–118.
[27] Sun, C. T., Achenbach, J. D., and Herrmann, G., 1968, "Continuum Theory for a Laminated Medium," ASME J. Appl. Mech., **35**(3), pp. 467–475.
[28] Murakami, H., Maewal, A., and Hegemier, G. A., 1979, "Mixture Theory for Longitudinal Wave Propagation in Unidirectional Composites With Cylindrical Fibers of Arbitrary Cross Section—I: Formulation," Int. J. Solids Struct., **15**(4), pp. 325–334.
[29] Murakami, H., 1985, "A Mixture Theory for Wave Propagation in Angle-Ply Laminates Part 1: Theory," ASME J. Appl. Mech., **52**(2), pp. 331–337.
[30] Murakami, H., and Akiyama, A., 1985, "A Mixture Theory for Wave Propagation in Angle-ply Laminates, Part 2: Application," ASME J. Appl. Mech., **52**(2), pp. 338–344.
[31] Zhao, Y. P., and Wei, P. J., 2009, "The Band Gap of 1d Viscoelastic Phononic Crystal," Comput. Mater. Sci., **46**(3), pp. 603–606.
[32] Mukherjee, S., and Lee, E., 1978, "Dispersion Relations and Mode Shapes for Waves in Laminated Viscoelastic Composites by Variational Methods," Int. J. Solids Struct., **14**(1), pp. 1–13.
[33] Kohn, W., Krumhansl, J. A., and Lee, E. H., 1972, "Variational Methods for Dispersion Relations and Elastic Properties of Composite Materials," ASME J. Appl. Mech., **39**(2), pp. 327–336.
[34] Minagawa, S., and Nemat-Nasser, S., 1977, "On Harmonic Waves in Layered Composites," ASME J. Appl. Mech., **44**(4), pp. 689–695.
[35] Minagawa, S., Nemat-Nasser, S., and Yamada, M., 1981, "Finite Element Analysis of Harmonic Waves in Layered and Fiber-Reinforced Composites," Int. J. Numer. Methods Eng., **17**(9), pp. 1335–1353.
[36] Naciri, T., Navi, P., and Ehrlacher, A., 1994, "Harmonic Wave Propagation in Viscoelastic Heterogeneous Materials—Part I: Dispersion and Damping Relations," Mech. Mater., **18**(4), pp. 313–333.
[37] Aberg, M., and Gudmundson, P., 1997, "The Usage of Standard Finite Element Codes for Computation of Dispersion Relations in Materials With Periodic Microstructure," J. Acoust. Soc. Am., **102**(4), pp. 2007–2013.
[38] Wang, P., Shim, J. M., and Bertoldi, K., 2013, "Effects of Geometric and Material Nonlinearities on Tunable Band Gaps and Low-Frequency Directionality of Phononic Crystals," Phys. Rev. B, **88**(1), p. 014304.
[39] Guarin-Zapata, N., and Gomez, J., 2015, "Evaluation of the Spectral Finite Element Method With the Theory of Phononic Crystals," J. Comput. Acoust., **23**(2), p. 1550004.
[40] Wang, P., and Bertoldi, K., 2012, "Mechanically Tunable Phononic Band Gaps in Three-Dimensional Periodic Elastomeric Structures," Int. J. Solids Struct., **49**(19–20), pp. 2881–2885.
[41] Bayat, A., and Gordaninejad, F., 2014, "A Magnetically Field-Controllable Phononic Crystal," Act. Passive Smart Struct. Integr. Syst., **9057**, p. 905713.
[42] Shim, J., Wang, P., and Bertoldi, K., 2015, "Harnessing Instability-Induced Pattern Transformation to Design Tunable Phononic Crystals," Int. J. Solids Struct., **58**, pp. 52–61.
[43] Mousanezhad, D., Babaee, S., Ghosh, R., Mahdi, E., Bertoldi, K., and Vaziri, A., 2015, "Honeycomb Phononic Crystals With Self-Similar Hierarchy," Phys. Rev. B, **92**(10), p. 104304.
[44] Pennec, Y., Djafari-Rouhani, B., Vasseur, J., Khelif, A., and Deymier, P., 2004, "Tunable Filtering and Demultiplexing in Phononic Crystals With Hollow Cylinders," Phys. Rev. E, **69**(4 Pt. 2), p. 046608.
[45] Yang, W.-P., Wu, L.-Y., and Chen, L.-W., 2008, "Refractive and Focusing Behaviours of Tunable Sonic Crystals With Dielectric Elastomer Cylindrical Actuators," J. Phys. D: Appl. Phys., **41**(13), p. 135408.
[46] Haque, A. B. M. T., and Shim, J., 2016, "On Spatial Aliasing in the Phononic Band-Structure of Layered Composites," Int. J. Solids Struct., **96**(1), pp. 380–392.
[47] Hussein, M. I., and Frazier, M. J., 2010, "Band Structure of Phononic Crystals With General Damping," J. Appl. Phys., **108**(9), p. 093506.
[48] Daraio, C., Nesterenko, V., Herbold, E., and Jin, S., 2006, "Tunability of Solitary Wave Properties in One-Dimensional Strongly Nonlinear Phononic Crystals," Phys. Rev. E, **73**(2 Pt. 2), p. 026610.
[49] Maldovan, M., and Thomas, E. L., 2009, *Periodic Materials and Interference Lithography for Photonics, Phononics and Mechanics*, Wiley-VCH, Weinheim, Germany.
[50] Graff, K. F., 1991, *Wave Motion in Elastic Solids*, Dover Publications, Mineola, NY.
[51] Birkhoff, G., and MacLane, S., 1977, *A Survey of Modern Algebra*, 4th ed., Macmillan Publishing, New York.
[52] Bracewell, R. N., 2003, *Fourier Analysis and Imaging*, Kluwer Academic/Plenum Publishers, New York.
[53] Brillouin, L., 1946, *Wave Propagation in Periodic Structures: Electric Filters and Crystal Lattices*, McGraw-Hill, New York.
[54] Backus, G. E., 1962, "Long-Wave Elastic Anisotropy Produced by Horizontal Layering," J. Geophys. Res., **67**(11), pp. 4427–4440.
[55] Khelif, A., Aoubiza, B., Mohammadi, S., Adibi, A., and Laude, V., 2006, "Complete Band Gaps in Two-Dimensional Phononic Crystal Slabs," Phys. Rev. E, **74**(4 Pt. 2), p. 046610.
[56] Vasseur, J. O., Hladky-Hennion, A.-C., Djafari-Rouhani, B., Duval, F., Dubus, B., and Pennec, Y., 2007, "Waveguiding in Two-Dimensional Piezoelectric Phononic Crystal Plates," J. Appl. Phys., **101**(11), p. 114904.
[57] Vasseur, J. O., Deymier, P. A., Djafari-Rouhani, B., and Pennec, Y., 2008, "Absolute Forbidden Bands and Waveguiding in Two-Dimensional Phononic Crystal Plates," Phys. Rev. B, **77**(8), p. 085415.
[58] Cheng, Y., Liu, X. J., and Wu, D. J., 2011, "Temperature Effects on the Band Gaps of Lamb Waves in a One-Dimensional Phononic-Crystal Plate (L)," J. Acoust. Soc. Am., **129**(3), pp. 1157–1160.
[59] Mace, B. R., and Manconi, E., 2008, "Modelling Wave Propagation in Two-Dimensional Structures Using Finite Element Analysis," J. Sound Vib., **318**(4–5), pp. 884–902.
[60] Manconi, E., 2008, "The Wave Finite Element Method for 2-Dimensional Structures," Ph.D. thesis, University of Parma, Parma, Italy.
[61] Houillon, L., Ichchou, M. N., and Jezequel, L., 2005, "Wave Motion in Thin-Walled Structures," J. Sound Vib., **281**(3–5), pp. 483–507.
[62] Duhamel, D., Mace, B. R., and Brennan, M. J., 2006, "Finite Element Analysis of the Vibrations of Waveguides and Periodic Structures," J. Sound Vib., **294**(1–2), pp. 205–220.
[63] Mencik, J. M., and Ichchou, M. N., 2007, "Wave Finite Elements in Guided Elastodynamics With Internal Fluid," Int. J. Solids Struct., **44**(7–8), pp. 2148–2167.